First-principles investigation of rhodium hydrides under high pressure

Ziji Shao,[1,2] Defang Duan,[1,*] Liyuan Wang,[1] Hao Song,[1] Hongyu Yu,[1] Yansun Yao,[3] and Tian Cui[4,1,†]

[1]*State Key Laboratory of Superhard Materials, College of Physics, Jilin University, Changchun, 130012, People's Republic of China*

[2]*College of electronics and information, Hangzhou Dianzi University, Hangzhou, 310018 People's Republic of China*

[3]*Department of Physics and Engineering Physics, University of Saskatchewan, Saskatoon, Saskatchewan, Canada S7N 5E2*

[4]*School of Physical Science and Technology, Ningbo University, Ningbo, 315211, People's Republic of China*

(Received 24 November 2020; accepted 29 July 2021; published 10 August 2021)

Hydrogen-rich compounds are being extensively explored theoretically and experimentally as potential hydrogen storage materials. In this work, we predicted a hydrogen-rich compound rhodium trihydride (RhH_3) with a high volumetric hydrogen density of 212.5 g/L by means of *ab initio* calculations. The RhH_3 with *Pnma* symmetry is thermodynamically stable and accessible through synthesis above 40 GPa. The compound is dynamically and mechanically stable at ambient pressure. Further calculation suggests a probable dehydrogenation temperature T_{des} of 65 °C at ambient pressure with decomposition route to $Rh + H_2$. High volumetric hydrogen density and moderate dehydrogenation temperature place RhH_3 as one of the best hydrogen storage materials. Our work encourages the experimental synthesis of RhH_3 at high pressure.

DOI: 10.1103/PhysRevB.104.054110

I. INTRODUCTION

The exhaustion of conventional fossil fuels and alarming environmental problems prompt a rapid search for renewable energy sources. As a promising alternative, hydrogen fuel is promising for its abundance, efficiency, and friendliness to the environment. However, low storage capacity and safety issues for hydrogen-carrying materials are major obstacles to the practical use of hydrogen fuel. Compared to traditional methods for hydrogen storage (compacted gas or liquid), metal hydrides such as MgH_2 or $KAlH_4$ are safer and have high volumetric hydrogen density about 110 g/L and 53.2 g/L [1], which satisfy the ultimate target of 50 g/L set by the U.S. Department of Energy [2]. But, due to the strong bonding between the main-group metals and hydrogen, the hydrogen desorption temperatures T_{des} are outside the acceptable range for practical applications (above 300 °C for MgH_2 and 270 °C for $KAlH_4$) [3,4]. Since T_{des} is closely related to the decomposition enthalpy, lower T_{des} likely exists in metastable transition-metal hydrides with lower thermodynamical stabilities.

Group VIII elements (Fe, Co, Ni, Ru, Rh, Pd, Os, Ir, and Pt) all have low solubility of hydrogen under ambient conditions. However, under high pressure, many novel polyhydrides of group VIII elements have been discovered recently, both by theory and experiment, such as $FeH_{2,3,5}$ [5,6], $CoH_{2,3}$ [7,8] IrH_3 [9], and RhH_2 [10]. Through a systematic analysis of these hydrides, we found three pieces of key information: (i) Hydrogen absorption in transition metals has a higher limit under pressure than originally thought. Transition-metal elements like Fe, Co, and Ir are all capable of forming high hydrides. For instance, CoH_3, IrH_3, FeH_3, and FeH_5 were successfully synthesized through high-pressure experiments [5,6,9,11]. On the other hand, Rh as an element close to Ir and Co only have RhH and RhH_2 known, which leads to a further exploration for rubidium polyhydrides with higher hydrogen content. (ii) Transition-metal polyhydrides can be regarded as a prototypic hydrogen storage material with high volumetric hydrogen density. RhH_2 synthesized above 8 GPa has a rather high volumetric hydrogen density of about 163.7 g/L [10]. For cobalt polyhydrides, the volumetric hydrogen densities are even higher, 214 and 435 g/L [8,10]. (iii) Transition-metal hydrides that are thermodynamically accessible at high pressure are often metastable at ambient pressure. RhH_2 was reported to be experimentally recoverable to ambient pressure at 6.1 K with T_{des} about 150–270 K [10]. IrH_3 is also expected to be recoverable due to the slow kinetics formation and decomposition of IrH_3 [9]. The hexagonal close-packed $CoH_{0.6}$ and fcc CoH which synthesized above 7 GPa can remain metastable at atmospheric pressure [12]. From the analysis above, RhH_3 is very likely to exist under high pressure but metastable under the ambient pressure condition and is expected to be a promising hydrogen storage material.

Here, we systematically investigate the high-pressure phase diagram on the Rh-H system from 1 atm to 300 GPa and successfully predict a hydrogen-rich compound RhH_3 with *Pnma* symmetry above 40 GPa by first-principles calculation. When pressure is decreased to 1 atm, RhH_3 still remains dynamically and mechanically stable with high volumetric hydrogen density (212.5 g/L). This capacity places RhH_3 as one of the best hydrogen storage materials, meritorious for synthesis and further investigation for practicable usage.

II. COMPUTATIONAL METHODS

According to the previous investigation on Co-H and Ir-H systems, the highest stable stoichiometry is 1:3. In addition, we performed coarse variable-composition predictions with about 2000 structures at 100 GPa using USPEX and found only RhH_{1-3} being located on the convex hull. Therefore, we focused the exploration on stable compounds of RhH_n

*duandf@jlu.edu.cn

†cuitian@nbu.edu.cn

($n = 1$–4) at 1 atm, 2, 4, 5, 10, 20, 40, 50, 100, 200, and 300 GPa based on the fixed composition search implemented by USPEX [13,14] with system sizes from two to four formula units per cell. To examine the possible existence of superhydrides with higher hydrogen contents, the structural research of RhH_n ($n = 5$–8) at 100, 200, and 300 GPa were also carried out. In the evolutionary cycle, 60 structures were randomly created as the first generation in the evolution. Every subsequent generation was composed of the best 60% structures with the lowest enthalpy from the previous generation and new structures which were produced by variation operator heredity (50%), soft mutation (20%), transmutation (10%), and 20% random structures. The simulation is considered converged once the best structure does not change for 20 generations. The structural geometry optimizations and electronic structure calculations were employed by the Vienna *Ab initio* Simulation Package (VASP) code [15] in the framework of density-functional theory. The electron-ion interactions were treated using the all-electron projector augmented wave potentials [16]. The exchange-correlation effects were described by the Perdew-Burke-Ernzerhof revised for solids parametrization of the generalized gradient approximation [17]. The valence electrons of H and Rh are $1s^1$ and $4d^8 5s^1$, respectively. To ensure that the calculated enthalpies are converged to better than 1 meV/atom, the plane-wave cutoff energy of 700 eV was employed with the energy and force convergence criteria of 10^{-7} eV and 0.005 eV Å^{-1}. The k-point grid spacing of $2\pi \times 0.03$ Å^{-1} and $2\pi \times 0.025$ Å^{-1} were used in calculations of enthalpies and electronic properties, respectively. Phonon calculations and zero-point energies (ZPE) were performed by the PHONOPY code using a finite displacement approach [18,19]. In structural optimizations and electronic structures calculations, the spin-polarized were included. Electron-phonon couplings were carried out within the framework of the linear-response theory as implemented in the QUANTUM ESPRESSO program [20]. A kinetic energy cutoff is set to be 80 Ry after the convergence tests. Norm–conserving pseudopotentials for H and Rh were chosen. The q–points sampling meshes of RhH_2-*Fm*-3*m*, RhH_2-$P2_1/m$, RhH_2-*Cmcm,* and RhH_3-*Pnma* were $6 \times 6 \times 6$, $2 \times 4 \times 4$, $4 \times 4 \times 4$, and $4 \times 4 \times 2$, respectively. The k-points meshes are $24 \times 24 \times 24$, $12 \times 24 \times 24$, $24 \times 24 \times 24$, and $16 \times 16 \times 8$, correspondingly.

III. RESULTS AND DISCUSSION

A. Stabilities and structures

The formation enthalpies (ΔH_f) of all predicted RhH_n ($n = 1$–4) are depicted through thermodynamic convex hull construction at selected pressures [Fig. 1(a)]. In order to examine the stabilization of the superhydrides, the stoichiometries with higher hydrogen contents $RhH_{5,6,7,8}$ are also taken into consideration at 100, 200, and 300 GPa. The convex hull of RhH_m ($m = 1$–8) at 100, 200, and 300 GPa are constructed (see Fig. S1 of the Supplemental Material [21]). In constructing the convex hull, the known structures of *Fm*-3*m* for Rh [10] and $P6_3/m$, $C2/c$, and *Cmca* for H_2 [22] are used as references. In addition to reproducing the experimentally known RhH and RhH_2, the structure search uncovers a previously unreported RhH_3 with *Pnma* space group, found to be stable above 40 GPa.

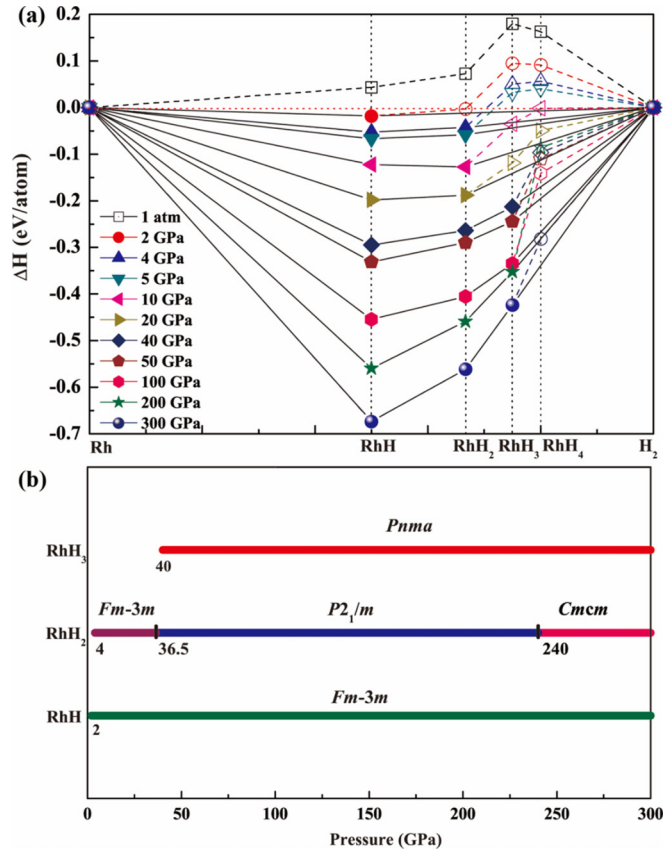

FIG. 1. (a) Convex hulls of the Rh-H system with respect to elemental Rh and H_2 from 1 atm to 300 GPa. The compounds located on the solid lines are thermodynamically stable. (b) The pressure-composition phase diagram of Rh-H system under high pressure.

No rhodium hydrides can form from elements at ambient conditions [10]. Our calculation shows that RhH and RhH_2 become thermodynamically stable at 2 and 4 GPa, respectively, which match well with the previous experimental study in which RhH and RhH_2 were synthesized at 4 and 8 GPa [10]. The predicted structures and corresponding pressure range of stability are shown in the pressure-composition phase diagram of Rh-H system from 1 atm to 300 GPa [Fig. 1(b)]. No phase transitions are found in RhH and RhH_3 in the entire investigated pressure range. RhH_2 is predicted to have two phase transitions at 36.5 and 240 GPa, respectively.

The predicted stable structures are presented in Fig. 2 and detailed structure parameters are provided in the Supplemental Material (Table SI) [21]. Consistent with experimental results [10,23], in *Fm*-3*m*-RhH and *Fm*-3*m*-RhH_2 [Figs. 2(a) and 2(b)], the Rh atoms located at the 4*a* Wyckoff positions form a face-centered cubic (fcc) sublattice, while H atoms fill the octahedral and tetrahedral voids. Upon increasing the pressure, *Fm*-3*m* phase of RhH_2 is predicted to transform to $P2_1/m$ phase at 36.5 GPa [Fig. 2(c)]. In this structure, Rh atoms are connected into individual rectangle sheets with the closest Rh-Rh distance of about 2.64 Å at 100 GPa. The Rh sheets are with the *ABAB* stacking sequence along the *a* axis with atomic H intercalated. When the pressure reaches

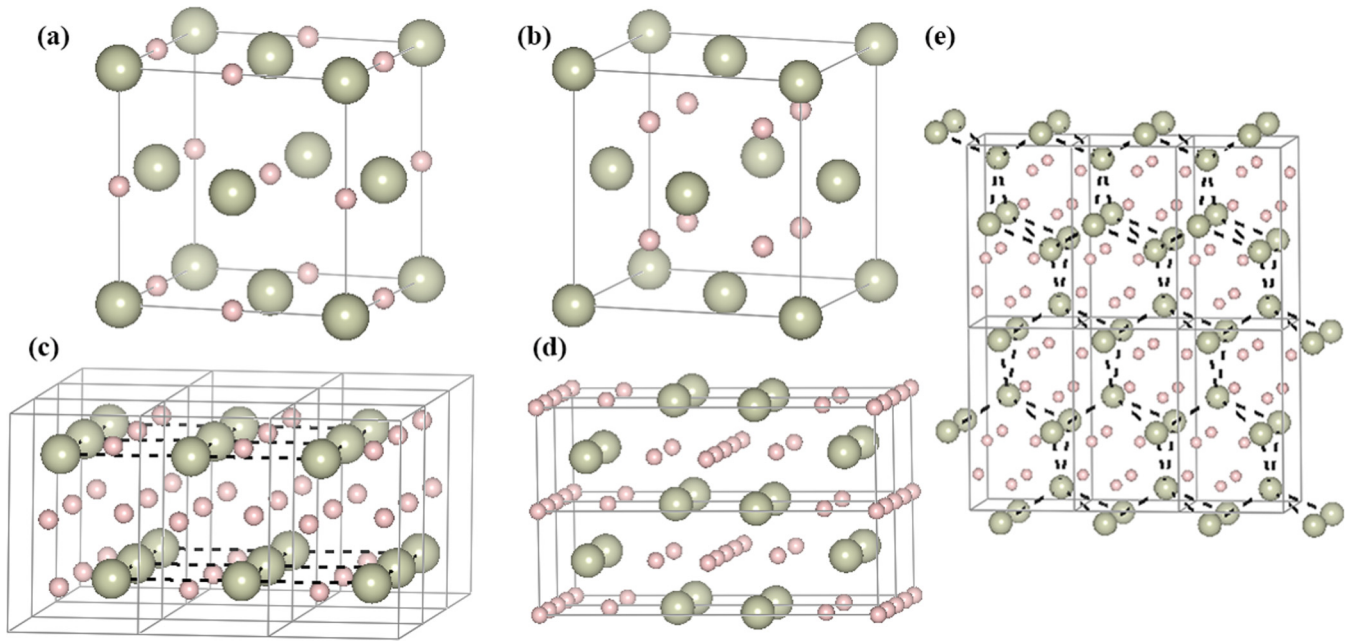

FIG. 2. The crystal structures of (a) *Fm*-3*m*-RhH, (b) *Fm*-3*m*-RhH_2, (c) $P2_1/m$-RhH_2, (d) *Cmcm*-RhH_2,and (e) *Pnma*-RhH_3. The big gray balls represent Rh atoms and small pink balls represent H atoms.

240 GPa, the $P2_1/m$ phase is predicted to transform to *Cmcm* phase [Fig. 2(d)]. The Rh atoms in *Cmcm*-RhH_2 are located at 4*c* sites and H atoms occupy the 4*c* and 4*a* sites. In addition to causing phase transition, the effect of pressure also includes increasing the hydrogen content. A hydrogen-rich rhodium trihydride RhH_3 with space group *Pnma* is revealed above 40 GPa which maintains the stability until at least 300 GPa. In this structure, the Rh atoms are hexaconnected (dashed line) and H atoms are distributed in the triangular prism interstices of Rh sublattices [Fig. 2(e)]. This structure is isostructural to the previously predicted *Pnma*-IrH_3 [9].

Learning from the experimental synthesis of Fe, Co, Rh, and Ir hydrides, the changes in symmetry may result in high-energy barriers. For Co and Rh in fcc lattice, only 4 GPa is required for the formation of fcc CoH and RhH, 8 GPa and 45 GPa for fcc RhH_2 and CoH_2 at room temperature, respectively [8,10]. But, for Fe in body-centered cubic and Ir in fcc, the formation of corresponding hydrides induces symmetry changes (tetragonal and simple cubic symmetries), and therefore require high-temperature conditions [5,6,9]. As for the *Pnma*-RhH_3 in our prediction, Rh adopts an orthorhombic sublattice instead of the cubic one in pure Rh. Thus, the significant change in symmetry will increase the energy barrier for the formation of RhH_3, which may require laser heating under pressure.

B. Equation of states

By fitting the pressure as a function of volume to the third-order Birch-Murnaghan equation of state (EOS) [24],

$$P = \frac{3}{2}B_0\left[\left(\frac{V_0}{V}\right)^{7/3} - \left(\frac{V_0}{V}\right)^{5/3}\right] \times \left\{1 + \frac{3}{4}(4 - B_0') \times \left[\left(\frac{V_0}{V}\right)^{2/3} - 1\right]\right\},$$

the EOS of Rh, and RhH_x ($x = 1$–3) are determined (Fig. 3). The equilibrium volumes at zero pressure (V_0), bulk modulus (B_0), and their pressure derivatives (B_0') are listed in Table I. Our calculation has a very good agreement with the values previously reported in experiments and calculations. The calculated lattice constant a_0 for Rh and RhH are 3.799 and 4.008 Å, which agree well with the experimental value of 3.803 and 4.010 Å [2]. The EOS of Rh and RhH_x ($x = 1$–3) are presented in Fig. 3 along with experimental data [10]. In the low-pressure range from 1 atm to 30 GPa, the volume expansions are 9.2 and 15.3 $Å^3$ in the staged absorption of hydrogen atoms (fcc-Rh→fcc-RhH→fcc-RhH_2), which are in good agreement with the experimental values [10] (9.9 and 15.4 $Å^3$). In the high-pressure range from 30 to 300 GPa, our prediction provides two suggestions for future experiments on high-pressure rhodium hydride. First, RhH_2 will likely experience two first-order phase transitions ($Fm{-}3m \rightarrow P2_1/m \rightarrow Cmcm$) with the volume reduction of 2.03 and 0.5 $Å^3$, respectively. Second, the formation of *Pnma*-RhH_3 will bring about 11.6 $Å^3$ volume increase at 40 GPa compared with $P2_1/m$-RhH_2 at the same pressure.

C. Electronic structures

Given that no electron accumulation is found in spaces between Rh and H by electronic localization functions (ELFs) as shown in Fig. 4, Bader charge analysis in Table SII therefore shows a direct charge transfer between Rh and H atoms in Rh-H solids. For *Fm*-3*m*-RhH, *Fm*-3*m*-RhH_2, $P2_1/m$-RhH_2, and *Pnma*-RhH_3 at 2, 4, 40, 250, and 40 GPa, each Rh on average loses about 0.05–0.2 e^- to H atoms. For *Cmcm*-RhH_2 at 250 GPa, each Rh atom on average gains about 0.006 e^- from H atoms. The ELF and Bader charge analysis show that the interactions between H and Rh atoms have slight ionic character. The spin polarization of Rh-H system is also taken

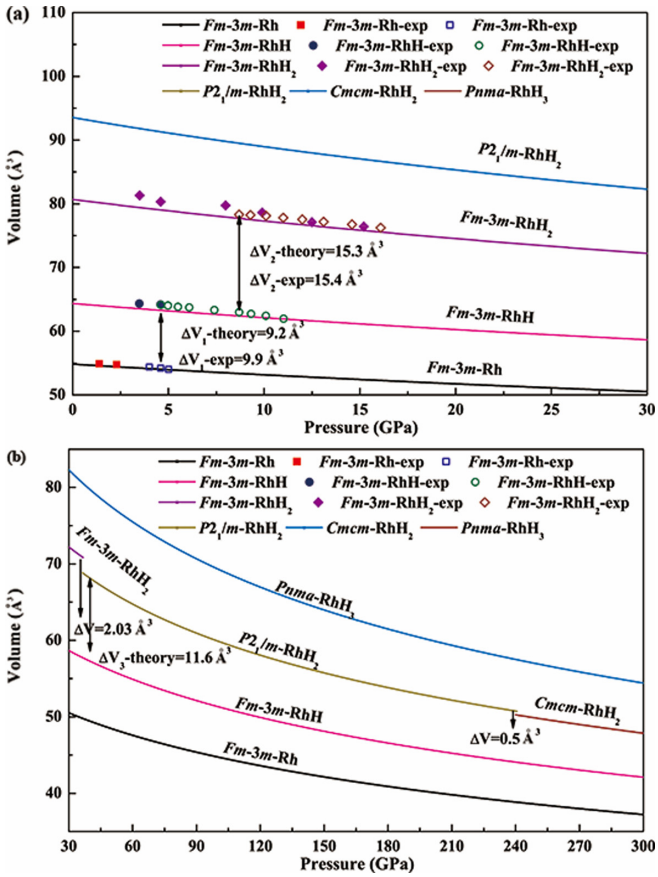

FIG. 3. EOS of Rh, RhH, RhH_2, and RhH_3 in the pressure range of (a) 0–30 and (b) 30–300 GPa. The results of our calculation are shown in solid lines and experimental data are represented by dots [10].

into consideration. According to our calculation, only RhH is magnetic. The magnetic moment of RhH is calculated to be 0.325 μ_B at 5 GPa, which is in agreement with other theoretical value of 0.45 μ_B [25]. The spin-polarized electronic band structure and electronic density of states (DOS) of RhH at 5 GPa are depicted in Figs. S3(a) and S3(b). The splitting between the spin-up and spin-down channels near the Fermi level induces magnetic moments. Partial electronic density of states indicates that the DOS at the Fermi level is dominated by Rh and magnetism of RhH mainly arises from the *d* electrons of Rh. All predicted rhodium hydrides are calculated metallic.

TABLE I. Zero-pressure volume V_0 (Å^3), bulk modulus B_0 (GPa), and pressure derivative of bulk modulus B_0' obtained from the equation of state by Birch-Murnaghan fit for Rh, RhH, RhH_2, and RhH_3.

Structure	V_0 (Å^3)	B_0 (GPa)	B_0'
Fm-3*m*-Rh	54.83	299.4	4.9
Experimental data [28]	55.00	270	
Other calculation [29]	59.05	245.1	
Fm-3*m*-RhH	64.35	261.4	4.6
Experimental data [10]	64.48		
Other calculation [29]	67.42	230.9	
Fm-3*m*-RhH_2	80.68	212.2	4.4
Experimental data [10]	81.72	194.3	
Other calculation [29]	84.13	189.34	
$P2_1/m$-RhH_2	79.82	169.9	5.0
Cmcm-RhH_2	76.46	221.1	4.5
Pnma-RhH_3	93.54	179.8	4.1

D. Dynamic stabilities and superconductivities

The phonon band structures and partial phonon density of states (PHDOS) of *Fm*-3*m*-RhH, *Fm*-3*m*-RhH_2, $P2_1/m$-RhH_2, *Cmcm*-RhH_2, and *Pnma*-RhH_3 at different pressures are displayed in Fig. S3 in the Supplemental Material [21] and Fig. 5. Since no imaginary frequencies are found in the entire first Brillouin zone, all considered

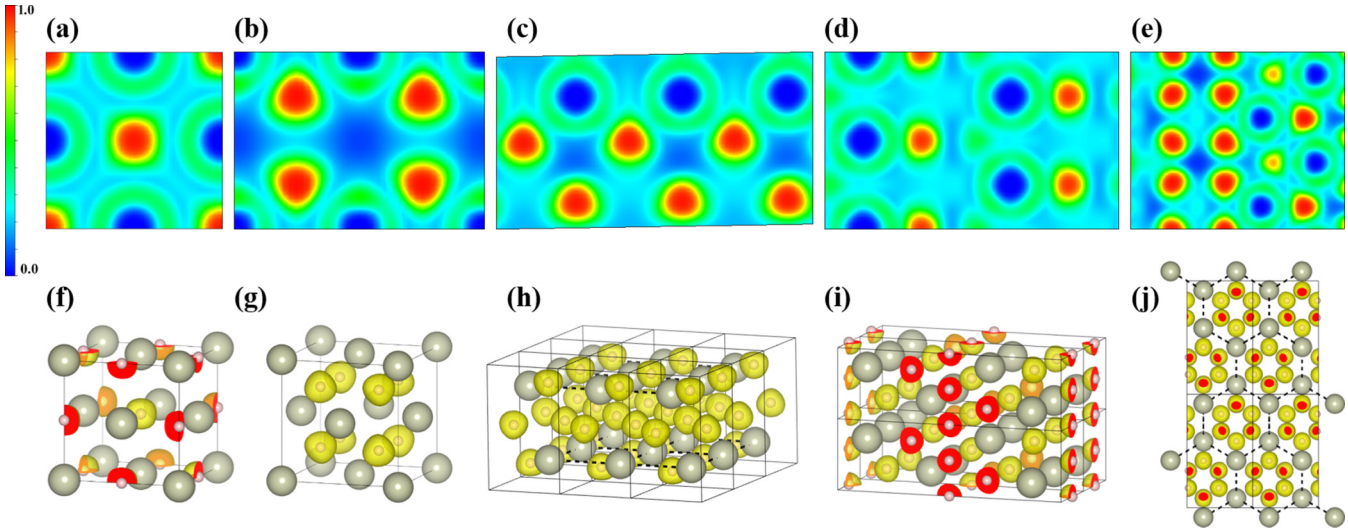

FIG. 4. The calculated 2D ELF of (a) *Fm*-3*m*-RhH at 2 GPa for the plane (001), (b) *Fm*-3*m*-RhH_2 at 4 GPa for the plane (0–11), (c) $P2_1/m$-RhH_2 at 40 GPa for the plane (010), (d) *Cmcm*-RhH_2 at 240 GPa for the plane (001), and (e) *Pnma*-RhH_3 at 50 GPa for the plane (103). (f)–(j) Their 3D ELFs. The isosurface is 0.6.

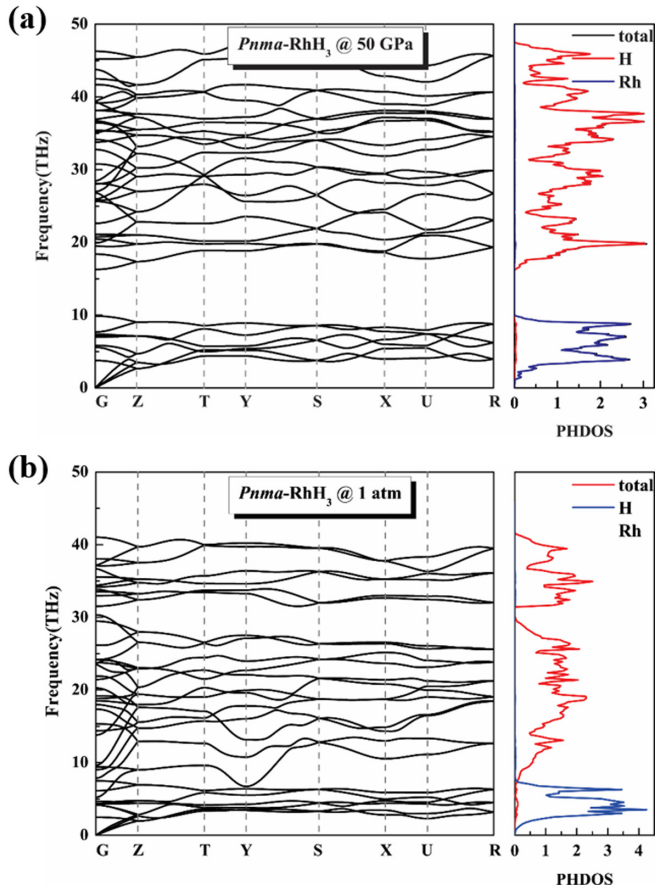

FIG. 5. The phonon band structures (left), total and PHDOS (right) of *Pnma*-RhH_3 at (a) 50 GPa and (b) 1 atm, respectively.

structures are dynamically stable. The different masses of two elements divide the phonon density of states into two parts: low-frequency and high-frequency ranges mainly correspond to the vibrations of Rh and H atoms, respectively.

Recently, the cobalt trihydride *Pm*-3*m*-CoH_3 was experimentally synthesized over 75 GPa, and the superconductive temperature T_c is calculated to be about 23 K [11]. Considering the metallic nature of Rh-H compounds, the superconductivity is investigated through the Allen-Dynes-modified McMillan equation [26] $T_c = \omega_{\log}/1.2\exp[-1.04(1+\lambda)/[\lambda-\mu^*(1+0.62\lambda)]]$. The calculated main superconducting characteristics and values are presented in Table SII. Due to the low contribution of H element to the DOS at the Fermi level $N(\varepsilon_F)$ and heavy mass of Rh atoms, the critical temperature (T_c) values of all R-H system are lower than 10 K.

E. Capability of hydrogen storage

Since the RhH_2 compound is considered as a potential hydrogen storage material with high volumetric hydrogen density (163.7 g/L) [10], the new RhH_3 compound with higher hydrogen content holds the same promise. Significantly, the calculated phonon band structure [Fig. 5(f)] and elastic constants (Table II) confirm that *Pnma*-RhH_3 is dynamically and mechanically stable at ambient pressure. The minimum

TABLE II. The calculated elastic constants (GPa) of *Pnma*-RhH_3 at 1 atm.

C_{11}	C_{22}	C_{33}	C_{44}	C_{55}	C_{66}	C_{12}	C_{13}	C_{23}
207.39	242.48	248.67	66.10	103.01	87.79	114.52	130.22	119.55

distances between hydrogen atoms in *Pnma*-RhH_3 at 40 GPa and 1 atm are calculated to be 1.62 and 1.80 Å, respectively, which are significantly larger than the typical bond length in H_2 molecules (0.74 Å). In *Pmna*-RhH_3, the hydrogen atoms are not paired, but present as isolated anions. The volumetric hydrogen density of *Pnma*-RhH_3 is calculated as large as 253.7 g/L at 50 GPa and 212.5 g/L at 1 atm, which indicates that *Pnma*-RhH_3 may be a potential hydrogen storage material. Different from metal hydrides naturally existing under normal conditions, *Pnma*-RhH_3 is thermodynamically metastable at 1 atm with a positive decomposition enthalpy. Herein, the decomposition of RhH_3 is an exothermic reaction with the decomposition enthalpy of about 0.172 eV/atom. According to the van't Hoff equation [27] at 1 atm, $T_d = \Delta H_d/\Delta S_d$, where the ΔH_d is the change of dehydrogenation enthalpy and ΔS_d is the change of reaction entropy of hydrogen which is about 130.7 J/K/mol; the calculated absolute value of T_{des} for RhH_3 is about 65 °C at ambient pressure. In the investigation of hydrogen storage materials, the capacity of hydrogen absorption and dehydrogenation of hydrogen are always trade-offs. Thus, high-pressure hydrides that are metastable under ambient conditions could be competitive candidates for hydrogen storage for its high volumetric hydrogen density and low decomposed temperature.

IV. CONCLUSION

In conclusion, we systematically investigated the structures, stability, superconductivity, and hydrogen storage ability of Rh-H compounds under high pressure by means of evolutionary algorithm USPEX and first-principle calculations. Two high-pressure phases $P2_1/m$ and *Cmcm* of RhH_2 are found at 36.5 and 240 GPa, respectively. Furthermore, the estimated superconducting critical temperature T_c of $P2_1/m$-RhH_2 reaches 6 K at 100 GPa. Rhodium polyhydride RhH_3 with *Pnma* symmetry is predicted to be stable above 40 GPa and remains so up to at least 300 GPa. Most importantly, the RhH_3 is found metastable at ambient pressure, giving it potential as practical hydrogen storage material with high volumetric hydrogen density of 212.5 g/L and decomposition temperature of 65 °C.

ACKNOWLEDGMENTS

This work was supported by the National Natural Science Foundation of China (Grants No. 11674122, No. 51632002, No. 520721881, No. 11974133, and No. 11804113), Program for Changjiang Scholars, Innovative Research Team in University (Grant No. IRT_15R23), and the Natural Sciences and Engineering Research Council of Canada (NSERC). Parts of the calculations were performed in the High Performance Computing Center (HPCC) of Jilin University and TianHe-1(A) at the National Supercomputer Center in Tianjin.

[1] Q. Lai, M. Paskevicius, D. A. Sheppard, C. E. Buckley, A. W. Thornton, M. R. Hill, Q. Gu, J. Mao, Z. Huang, H. K. Liu, Z. Guo, A. Banerjee, S. Chakraborty, and R. Ahuja, and K.-F. Aguey-Zinsou, ChemSusChem **8**, 2789 (2015).

[2] *Target Explanation Document: Onboard Hydrogen Storage for Light-Duty Fuel Cell Vehicles* (The United States Department of Energy, 2017), https://www.energy.gov/eere/fuelcells/downloads/target-explanation-document-onboard-hydrogen-storage-light-duty-fuel-cell.

[3] T. Sadhasivam, H.-T. Kim, S. Jung, S.-H. Roh, J.-H. Park, and H.-Y. Jung, Renewable Sustainable Energy Rev. **72**, 523 (2017).

[4] H. Wang, H. J. Lin, W. T. Cai, L. Z. Ouyang, and M. Zhu, J. Alloys Compd. **658**, 280 (2016).

[5] C. M. Pépin, A. Dewaele, G. Geneste, P. Loubeyre, and M. Mezouar, Phys. Rev. Lett. **113**, 265504 (2014).

[6] C. M. Pepin, G. Geneste, A. Dewaele, M. Mezouar, and P. Loubeyre, Science **357**, 382 (2017).

[7] L. Wang, D. Duan, H. Yu, H. Xie, X. Huang, Y. Ma, F. Tian, D. Li, B. Liu, and T. Cui, Inorg. Chem. **57**, 181 (2018).

[8] M. Wang, J. Binns, M.-E. Donnelly, M. Peña-Alvarez, P. Dalladay-Simpson, and R. T. Howie, J. Chem. Phys. **148**, 144310 (2018).

[9] T. Scheler, M. Marques, Z. Konopkova, C. L. Guillaume, R. T. Howie, and E. Gregoryanz, Phys. Rev. Lett. **111**, 215503 (2013).

[10] B. Li, Y. Ding, D. Y. Kim, R. Ahuja, G. Zou, and H.-K. Mao, Proc. Natl. Acad. Sci. USA **108**, 18618 (2011).

[11] M. Peña-Alvarez, B. Li, L. C. Kelsall, J. Binns, P. Dalladay-Simpson, A. Hermann, R. T. Howie, and E. Gregoryanz, J. Phys. Chem. Lett. **11**, 6420 (2020).

[12] V. E. Antonov, T. E. Antonova, V. K. Fedotov, T. Hansen, A. I. Kolesnikov, and A. S. Ivanov, J. Alloys Compd. **404**, 73 (2005).

[13] A. O. Lyakhov, A. R. Oganov, H. T. Stokes, and Q. Zhu, Comput. Phys. Commun. **184**, 1172 (2013).

[14] A. R. Oganov and C. W. Glass, J. Chem. Phys. **124**, 244704 (2006).

[15] G. Kresse and J. Furthmüller, Comput. Mater. Sci. **6**, 15 (1996).

[16] G. Kresse and D. Joubert, Phys. Rev. B **59**, 1758 (1999).

[17] J. P. Perdew, A. Ruzsinszky, G. I. Csonka, O. A. Vydrov, G. E. Scuseria, L. A. Constantin, X. Zhou, and K. Burke, Phys. Rev. Lett. **100**, 136406 (2008).

[18] K. Parlinski, Z. Q. Li, and Y. Kawazoe, Phys. Rev. Lett. **78**, 4063 (1997).

[19] A. Togo, F. Oba, and I. Tanaka, Phys. Rev. B **78**, 134106 (2008).

[20] P. Giannozzi, S. Baroni, N. Bonini, M. Calandra, R. Car, C. Cavazzoni, D. Ceresoli, G. L. Chiarotti, M. Cococcioni, and I. Dabo, J. Phys.: Condens. Matter **21**, 395502 (2009).

[21] See Supplemental Material at http://link.aps.org/supplemental/10.1103/PhysRevB.104.054110 for detailed structure parameters (Table SI), the results of Bader charge analysis (Table SII), and superconductive parameters (Table SIII), convex hull of RhH_n ($n = 1$–8) at 100, 200, and 300 GPa with ZPE (Fig. S1), band structure with spin polarization of RhH (Fig. S2), phonon dispersion curves (Fig. S3), and band structures of RhH_2 and RhH_3 at different pressures (Fig. S4).

[22] C. J. Pickard and R. J. Needs, Nat. Phys. **3**, 473 (2007).

[23] M. Tkacz, J. Chem. Phys. **108**, 2084 (1998).

[24] F. Birch, J. Geophys. Res. Solid Earth **83**, 1257 (1978).

[25] X. Cui, J.-T. Wang, X.-X. Liang, and G.-Z. Zhao, Solid State Commun. **149**, 322 (2009).

[26] P. B. Allen and R. C. Dynes, Phys. Rev. B **12**, 905 (1975).

[27] M. V. Lototskyy, I. Tolj, L. Pickering, C. Sita, F. Barbir, and V. Yartys, Prog. Nat. Sci.: Mater. Int. **27**, 3 (2017).

[28] M. J. Mehl and D. A. Papaconstantopoulos, Phys. Rev. B **54**, 4519 (1996).

[29] G. Pan, C. Hu, P. Zhou, F. Wang, Z. Zheng, and B. Liang, J. Mater. Res. **29**, 1334 (2014).